Supplementary Information:

Two Heteronuclear Dipolar Results at the Price of One: Quantifying Na/P Contacts in Phosphosilicate Glasses and Biomimetic Hydroxy-Apatite

Baltzar Stevensson, Renny Mathew, Yang Yu, and Mattias Edén*

Physical Chemistry Division, Department of Materials and Environmental Chemistry,

Arrhenius Laboratory, Stockholm University, SE-106 91 Stockholm, Sweden

*Corresponding author. E-mail: *mattias.eden@mmk.su.se*

Contents

S1. Materials and Methods

S1.1. Sample Preparations and Characterizations

Each of the eight Na_2O–CaO–SiO_2–P_2O_5 glasses were prepared with a standard melt-quench procedure in an electric furnace, using ball-milled mixtures of NaH_2PO_4 (99.99%; Merck), and Na_2CO_3 (99.9%), $CaCO_3$ (99.9%), and SiO_2 (99.99%) from ChemPur. Each 6.0 g batch incorporated paramagnetic doping by 0.1 wt% Fe_2O_3 and was pre-heated in a Pt crucible at 950 °C for 4 h to ensure complete carbonate removal. Depending on the glass composition, the temperature was then raised to a value in the range of 1350–1620 °C, held there for 4 h and then quenched by immersing the bottom of the crucible in water.

Scanning electron microscopy (SEM) in back-scatter mode evidenced homogeneous glasses, while powder X-ray diffraction (XRD) gave no signs of crystalline impurities above an estimated lower detection limit of ≈1%. SEM coupled with energy-dispersive X-ray spectroscopy (EDS) revealed a good agreement between the nominally batched and the analyzed glass compositions (see Table **S1**), with the deviations remaining within the uncertainty of the measurements. Further details about the glass synthesis and basic characterizations are given in our recent reports [S1,S2].

The "S90" mesoporous bioactive glass (MBG) has a nominal composition 10CaO–90SiO_2 and was prepared as described in [S3]. The "S90sbf" specimen resulted after soaking 600 mg of MBG powder in 1.0 L of simulated body fluid (SBF) for a period of 15 days (courtesy of Dr. Isabel Izquierdo-Barba and Prof. María Vallet-Regí at the Universidad Complutense de Madrid). This procedure also followed that of ref. [S3], except for the MBG loading, i.e., its mass per unit volume of SBF. The element composition was analyzed by Medac Ltd. (UK), which resulted in the cation composition (6.6; 30.7; 2.9; 0.11) wt% for (Ca; Si; P; Na), respectively.

The polycrystalline Na_3PO_4 (99.96% purity) and NaH_2PO_4 (99.99% purity) samples were used as received from Sigma-Aldrich and Merck, respectively.

S1.2. Solid-State NMR

The NMR experimentation was performed with a Bruker Avance-III spectrometer at $B_0 = 9.4$ T that corresponds to a ^{1}H Larmor frequency of −400.07 MHz. Finely ground samples were filled in 4 mm zirconia rotors. They were spun at the MAS rate $\nu_r = (14000 \pm 2)$ Hz in a triple-resonance Bruker NMR probehead, except for the ^{31}P{^{23}Na} REAPDOR experiments on the S90sbf sample that employed $\nu_r = (7000 \pm 2)$ Hz. Furthermore, additional ^{31}P{^{23}Na} REAPDOR experiments were acquired at $\nu_r = 10.00$ kHz for Na_3PO_4. ^{31}P and ^{23}Na shifts are quoted relative to 85% H_3PO_4 and 0.1 M NaCl(aq), respectively.

The ^{23}Na nutation frequencies (ν_1^{Na}) stated below were calibrated by using 0.1 M NaCl(aq), whereas those for ^{31}P were determined directly from each solid powder. All ^{23}Na{^{31}P} REDOR experimentation involved central-transition-selective ^{23}Na pulses operating at $\nu_1^{\mathrm{Na,CT}}$=16 kHz, corresponding to 90°/180° pulse-lengths of 15.6/31.3 μs. The ^{31}P 180° recoupling pulses were 6.9 μs for both REDOR and REAPDOR NMR acquisitions. All heteronuclear NMR implementations cycled the rf phases of the 180° recoupling pulses according to the XY8 or XY16 scheme to minimize rf errors [S4]. Each dephasing data-set was sampled at each *even integral* multiple of τ_r, i.e., not solely at completed XYn cycles.

The adiabatic passage pulse for REAPDOR operated at $\nu_1^{\mathrm{Na}} = 75$ kHz and spanned $\tau_r/3$, i.e., 24 μs (33 μs at ν_r=10.0 kHz) and 48 μs for the experimentation on the glasses and S90sbf, respectively. The REAPDOR experiments started from transverse ^{31}P magnetization by applying a 90° rf pulse, except for those of the H-bearing NaH_2PO_4 and S90sbf samples that utilized ramped ^{1}H⟶ ^{31}P cross-polarization (CP) at the modified Hartmann-Hahn condition $\nu_1^{\mathrm{H}} = \nu_1^{\mathrm{P}} + \nu_r$, with $\nu_1^{\mathrm{P}} = (40 \pm 2)$ kHz throughout. The contact interval was 1.0 ms (NaH_2PO_4) or 6.0 ms (S90sbf), while CW decoupling

at $\nu_1^{\mathrm{H}} = 70$ kHz was applied during all time-segments devoid of S-pulses. A relatively long contact interval was utilized for the experimentation on S90sbf to emphasize the ^{31}P NMR signals from the *ordered* apatite component relative to its amorphous precursor phase (see ref. [S5] for further details).

Saturation-recovery blocks were used prior to relaxation delays of 20 s and 4 s in the recording of each ^{31}P$\{^{23}$Na$\}$ REAPDOR signal transient on the phosphosilicate glasses and S90sbf, respectively, whereas those for ^{23}Na$\{^{31}$P$\}$ REDOR employed 4 s for the glasses and 2 s for S90sbf. All REDOR experimentation furthermore utilized the RAPT technique [S6] to enhance the ^{23}Na CT magnetization and thereby the experimental sensitivity, where typically 40 pulse-blocks were employed with equal pulse/interpulse durations of 0.55 μs and ν_1^{Na} =75 kHz. The REDOR/REAPDOR NMR data were acquired in 3–4 blocks per phosphosilicate glass sample and τ_{rec} value, each involving 16–64 accumulated signal transients, depending on the particular experimental protocol and glass specimen. The corresponding REDOR data collection for S90sbf utilized 4 blocks, each comprising 1024 signal transients, whereas that for REAPDOR involved 8–12 blocks of 128 transients (except for the longest recoupling periods where 256–512 transients and 8 blocks were utilized). These independent experimental data sets were separately processed, integrated, and numerically fitted to derive the dipolar second-moment of each sample, whose reported average M_2-value and associated uncertainty were calculated from those of the various blocks.

Most of these heteronuclear recoupling NMR acquisitions were very time-consuming. The durations of the ^{23}Na$\{^{31}$P$\}$ REDOR experiments for each phosphosilicate glass ranged over 7–14 h, whereas the corresponding ^{31}P$\{^{23}$Na$\}$ REAPDOR data-collection required between 24 h and 48 h per sample. On the other hand, each REDOR and REAPDOR NMR acquisition on S90sbf demanded ≈60 h. The markedly longer REDOR experimental time relative to those of the phosphosilicate glasses stems from the minute amount of Na in the S90sbf sample (0.12 at%), relative to those of the glasses (11–17 at%).

S1.3. MD Simulations

Classical atomistic MD simulations were performed with the DLPOLY3 package [S7,S8] for NVT ensembles of {Na, Ca, Si, P, O} atoms placed in a cubic box with periodic boundary conditions, so as to match the experimental glass density [S1,S2] and the *nominal* element composition specified in Table **S1**. The computations involved a polarizable shell-model potential, where each cation carries its full formal charge, while the O^{2-} species are represented by core (O_C) and shell (O_S) units, coupled by a 300 THz harmonic oscillator and bearing charges of z_C=+0.8482e and z_S=−2.8482e, respectively [S9]. A Buckingham potential parameterized all short-range O_S–O_S and cation–O_S pair interactions that were evaluated out to 0.8 nm [S9]. Long-range Coulombic interactions were calculated by a smoothed particle mesh Ewald summation [S8] with a 1.2 nm real-space cut-off and an accuracy of 10^{-6}.

Each melt-quench protocol started from a random atom configuration that was "equilibrated" for 100 ps at 3500 K, followed by a 10 K/ps cooling procedure down to 300 K in steps of 10 ps, and a subsequent equilibration for 200 ps, from which 7500 samples of the last 150 ps were used in the analysis. This procedure was completed 2–4 times with different (random) initial atom configurations for each glass composition, from which the average value and uncertainty of the reported dipolar second moments were derived. By exploiting the periodic boundary conditions, fully converged M_2(Na–P) and M_2(P–Na) values were calculated by accounting for all atoms within several nanometers from the central site. We refer to [S1,S2] for further details about the MD modeling procedures.

S2. ^{23}Na$\{^{31}$P$\}$ REDOR Data Analysis

When extracting dipolar second moments from experimental REDOR data, it has been recommended [S10,S11] to restrict the experimental dephasing range to $\Delta S/S_0 \lesssim 0.2$ and employ solely the leading term ($\sim M_2(\mathrm{S–I})\tau_{\mathrm{rec}}^2$) in the following expression

$$\Delta S/S_0 = \frac{4A}{I(I+1)} M_2\,(\text{S–I})\,\tau_{\text{rec}}^2\left\{1 - B{\cdot}M_2\,(\text{S–I})\,\tau_{\text{rec}}^2\right\}, \tag{S1}$$

where $A = 1$ and $B = 10/[7I(I+1)] \approx 1.904$ for $I = 1/2$. Despite that the numerical fitting accuracy generally improves when the number of measurements increases, the data-set $\{\tau_{\text{rec}}, \Delta S/S_0\}$ employed for fitting must be restricted to short recoupling periods because Eq. (S1) is a Taylor expansion (truncated at the second term) of an exact solution for an *isolated* S–I spin-*pair* [S12], while the impact on the heteronuclear recoupling from I–I dipolar interactions is not accounted for [S13]. The approximation of the REDOR dephasing dynamics for SI_n clusters expressed as a superposition of S–I spin-pair responses works well in the limit $\Delta S/S_0 \rightarrow 0$, but the quality of this approximation degrades rapidly as the recoupling interval grows. While the higher-order expansion terms differ for SI and SI_n systems (the latter comprising geometry-dependent contributions [S13]), we included the term $\sim \tau_{\text{rec}}^4$ in our analysis, owing to an observed lower drop of the best-fit M_2-values when $\Delta S/S_0$ data associated with longer τ_{exc} periods are included, relative to the scenario of only employing the leading term in the expansion [Eq. (S1)]. Nevertheless, a minor reduction of the best-fit M_2-values is observed when τ_{rec} increases; see Table **S2** that lists the best-fit REDOR results obtained from the glass series when including all experimental data with $\Delta S/S_0 \leq 0.05$, ≤ 0.10, and ≤ 0.20, respectively. All M_2(Na–P) values presented and discussed in the main text were extracted from the range $\Delta S/S_0 \leq 0.10$. Figure **S3** displays a selection of dephasing curves.

Besides that an M_2(S–I) value may be underestimated due to the fundamental limitations of the two-spin approximation [Eq. (S1)], the best-fit second moments depend on other systematic errors originating from experimental obstacles, such as inhomogeneity of the rf field of the 180° recoupling pulses and spreads in S–I dipolar interactions from the structural disorder stemming from the amorphous nature of glasses [S10,S13–S15]. To assess the accuracy of our REDOR-derived M_2(Na–P) values, we collected data from two crystalline phosphate model samples under identical experimental conditions as for the glasses. The Na_3PO_4 and NaH_2PO_4 structures feature five [S16,S17] and two [S18,S19] crystallographically inequivalent Na sites, respectively. The ^{23}Na NMR spectra resolution allowed for separately deriving the second moments for the NaI and NaII sites of NaH_2PO_4, whereas the reported M_2(Na–P) value for Na_3PO_4 constitutes an average over all its Na sites. Figure **S4** provides the experimental dephasing curve for Na_3PO_4 and Table **S2** lists all experimentally extracted M_2(S–I) values, as well as those calculated from the diffraction-derived atom coordinates. All three estimated dipolar second moments reveal very similar degrees of underestimations compared with their theoretical counterparts, where the $M_2^{\text{exp}}/M_2^{\text{theo}}$ ratios fall in the range 0.68–0.70 (see Table **S2**). Noteworthy, the M_2^{theo} data presented herein constitutes fully converged values that were calculated over long distances of several nm for each crystal structure. Literature reports of analogous $M_2^{\text{exp}}/M_2^{\text{theo}}$ ratios frequently employs much shorter cut-off radii in the calculations (e.g., for Na_3PO_4 [S14]), thereby also apparently improving the agreement between the NMR/diffraction-derived M_2 data.

S3. ^{31}P{^{23}Na} REAPDOR Data Analysis

As opposed to the REDOR NMR protocol that implements detection of the quadrupolar nucleus ^{23}Na, the rf pulsing on the ^{23}Na spins in the REAPDOR applications complicates quantitative second-moment estimates due to the interference from first-order quadrupolar interactions [S20,S21]. However, the results are expected to be reasonably insensitive to the precise ^{23}Na quadrupolar parameters for our experimental conditions, because the mean ^{23}Na quadrupolar products $C_{Q\eta} = C_Q\sqrt{1+\eta^2/3}$ are relatively low for these glasses ($C_{Q\eta} \approx$1.6 MHz). These values were estimated by fitting ^{23}Na MAS NMR spectra recorded at two distinct external fields; Fig. **S5** shows one example. The ^{23}Na NMR results will be discussed in detail elsewhere. Nevertheless, the parameter A of Eq. (S1) is not *a priori* known for REAPDOR when applied to multi-spin SI_n systems. For well-ordered structures,

whose chemical shift and quadrupolar tensor parameters are known, the extraction of accurate M_2-values from REAPDOR NMR data may be accomplished through numerically exact spin dynamics calculations. Unfortunately, such an approach looses its accuracy for disordered structures, where spreads of the NMR-parameters and a generally absent knowledge of their precise distribution-widths hamper the analyses. Such hurdles apply to the present glasses. Yet, experimental M_2(P–Na) values extracted from the following two simple and straightforward analysis protocols revealed a remarkably good mutual agreement:

(*i*) We determined the parameter value A of Eq. (S1) by utilizing the REAPDOR results of the crystal structure of Na_3PO_4 (see Fig. **S4**), whose dephasing data in the range $\Delta S/S_0 \lesssim 0.2$ was fitted to the *known* M_2^{calc}(P–Na) result that was computed from the XRD-derived atom coordinates. This yielded the empirically derived parameter A =1.468 of Eq. (S1) that was employed to fit the corresponding data of the phosphosilicate glasses. Figure **S6** provides a few ^{31}P{^{23}Na} REAPDOR dephasing curves, whereas Table **S2** lists the resulting best-fit M_2(P–Na) values. The successful application of the present data-correction approach is supported by the observation that Fig. **S6**(a) verifies very similar asymptotic dephasing values for long recoupling periods among the glass samples, as well as for the Na_3PO_4 model structure (Fig. **S4**), thereby justifying the use of one empirically derived value of A throughout the data fitting.

(*ii*) We also fitted the REAPDOR dephasing data to the "universal curve" proposed by Nimerovsky and Goldbourt [S22] for spin-*pairs*. In terms of the second moment, it reads

$$\Delta S/S_0 = \frac{3}{4}\left(1-\exp\left\{-\left(1.75\ b_{\mathrm{eff}}^{\mathrm{P-Na}}\cdot\tau_{\mathrm{rec}}\right)^2\right\}\right) = \frac{3}{4}\left(1-\exp\left\{-M_2\,(\mathrm{P–Na})\cdot(1.75\ \tau_{\mathrm{rec}})^2\right\}\right) \qquad \text{(S2)}$$

for the present {S=1/2; I=3/2} combination, where $b_{\mathrm{eff}}^{\mathrm{P-Na}}$ denotes the effective dipolar coupling constant. We utilized the range $\Delta S/S_0 \lesssim$0.20 in the numerical fitting of the glasses; note that the dephasing regime must be restricted because Eq. (S2) only applies strictly for the case of a two-spin system [in analogy of employing Eq. (S1)]. For instance, multi-spin effects manifest in that the asymptotic values ($0.8 \lesssim \Delta S/S_0 \lesssim 0.95$) observed herein are larger than the prefactor of 0.75 in Eq. (S2). We refer to [S22] for further discussions. Nevertheless, the excellent consistency observed between the M_2 (P–Na) data derived either from Eqs. (S1) or (S2) strongly suggests that both approaches are valid for analyzing REAPDOR NMR data from multi-spin systems in amorphous materials (see Fig. **S2**). This inference is further supported by the very good agreement between the two directly estimated M_2 (P–Na) data sets and their MD-generated, as well as REDOR-derived, counterparts (see Fig. **1**).

Table S1: Phosphosilicate Glass Compositions[a]

label	$a\mathrm{Na_2O}$	$b\mathrm{CaO}$	$c\mathrm{SiO_2}$	$d\mathrm{P_2O_5}$	$\rho_{\mathrm{Na}}/\mathrm{nm}^{-3}$	$\rho_{\mathrm{Ca}}/\mathrm{nm}^{-3}$	$\rho_{\mathrm{Si}}/\mathrm{nm}^{-3}$	$\rho_{\mathrm{P}}/\mathrm{nm}^{-3}$
$\mathrm{BG}_{2.0}(2.5)$	0.197(0.191)	0.257(0.258)	0.526(0.527)	0.020(0.024)	10.47	6.79	13.95	1.04
$\mathrm{BG}_{2.0}(2.9)$	0.165(0.151)	0.215(0.206)	0.600(0.623)	0.020(0.020)	8.47	5.55	15.48	1.07
$\mathrm{BG}_{2.6}(2.1)$	0.244(0.229)	0.269(0.255)	0.461(0.486)	0.026(0.030)	12.86	7.11	12.21	1.38
$\mathrm{BG}_{2.6}(2.7)$	0.202(0.194)	0.222(0.214)	0.550(0.560)	0.026(0.032)	10.38	5.71	14.15	1.33
$\mathrm{BG}_{4.0}(2.5)$	0.209(0.193)	0.271(0.254)	0.480(0.509)	0.040(0.044)	10.77	7.00	12.43	2.10
$\mathrm{BG}_{4.0}(2.9)$	0.179(0.162)	0.233(0.226)	0.548(0.572)	0.040(0.040)	9.03	5.91	13.86	2.05
$\mathrm{BG}_{6.0}(2.1)$	0.221(0.207)	0.324(0.315)	0.395(0.412)	0.060(0.065)	11.39	8.36	10.17	3.09
$\mathrm{BG}_{6.0}(2.5)$	0.219(0.201)	0.287(0.274)	0.434(0.460)	0.060(0.065)	11.16	7.22	11.00	3.08

[a]To keep a consistent notation with our earlier and complementary reports on these phosphosilicate glasses, each specimen is labeled $\mathrm{BG}_p(\overline{N}^{\mathrm{Si}}_{\mathrm{BO}})$; the roles of the "silicate network connectivity" ($\overline{N}^{\mathrm{Si}}_{\mathrm{BO}}$) [S23] and $\mathrm{P_2O_5}$ content (p mol% $\mathrm{P_2O_5}$) are explained/discussed in our previous work [S1,S2]. The coefficients $\{a, b, c, d\}$ specify the *nominally* batched $a\mathrm{Na_2O}$–$b\mathrm{CaO}$–$c\mathrm{SiO_2}$–$d\mathrm{P_2O_5}$ oxide equivalent with $a+b+c+d=1$. Values within parentheses are SEM/EDS-analyzed compositions. ρ_E represents the number density of element E.

Table S2: Best-Fit Dipolar Second Moments[a]

label	M_2(Na–P)/(10^4 s^{-2}) REDOR(TE)[b]	M_2(P–Na)/(10^5 s^{-2}) REDOR-derived[c]	REAPDOR(TE)	REAPDOR(uni)
$BG_{2.0}(2.5)$	1.85-**1.59**-1.50	7.85	7.49	7.39
$BG_{2.0}(2.9)$	1.56-**1.40**-1.21	5.77	6.12	5.91
$BG_{2.6}(2.1)$	2.25-**2.18**-2.02	10.22	9.40	9.10
$BG_{2.6}(2.7)$	2.07-**1.92**-1.77	7.46	7.36	7.40
$BG_{4.0}(2.5)$	2.94-**2.95**-2.88	7.70	6.74	6.96
$BG_{4.0}(2.9)$	2.89-**2.79**-2.51	6.24	6.21	6.14
$BG_{6.0}(2.1)$	4.49-**4.49**-4.38	8.26	7.40	7.54
$BG_{6.0}(2.5)$	4.48-**4.36**-4.30	7.96	7.09	7.17
Crystalline Phosphates[d]				
Na_3PO_4	9.03±0.10—12.961			14.58±0.05—19.74
NaH_2PO_4-NaI	6.85±0.08—10.368			
NaH_2PO_4-NaII	8.22±0.07—11.735			

[a]Dipolar second moments ("TE") obtained directly by fitting the experimental $\Delta S/S_0$ REDOR/REAPDOR NMR data to Eq. (S1). The REAPDOR dephasing curves were also fitted to the universal curve ("uni") of ref. [S22], i.e., Eq. (S2). Note that the M_2-values reported here are given in units of s^{-2}=Hz^2 that are commensurate with (effective) dipolar coupling constants in units of Hz. Most of the literature utilizes b_{eff} and M_2 data in units of rad s^{-1} and rad^2s^{-2}, respectively, although the latter is (unfortunately) often expressed as s^{-2} (i.e., with the rad^2 portion of the unit omitted). Multiplication of each M_2-value presented herein by the factor $4\pi^2$ yields the corresponding result in rad^2s^{-2}.

[b]Best-fit results obtained by restricting $\Delta S/S_0$ to the approximate ranges 0.05, 0.10 and 0.20, respectively. The bold-face numbers are those used for all remaining analysis.

[c]Calculated by feeding the M_2(Na–P) value obtained from REDOR through Eq. (2).

[d]Experimental M_2-values (left entries) obtained from polycrystalline powders of the as-indicated model phosphates, shown together with calculated results (right entries) by using the XRD-derived atom coordinates for the Na_3PO_4 [S16,S17] and NaH_2PO_4 [S18,S19] structures. In each case, the crystal structure reference data was obtained as an average over the two as-indicated independently reported crystal structures. The ratio between the NMR and XRD-derived M_2-estimates was employed to correct/calibrate the corresponding values of the phosphosilicate glasses, as described in sections **S2** and **S3**.

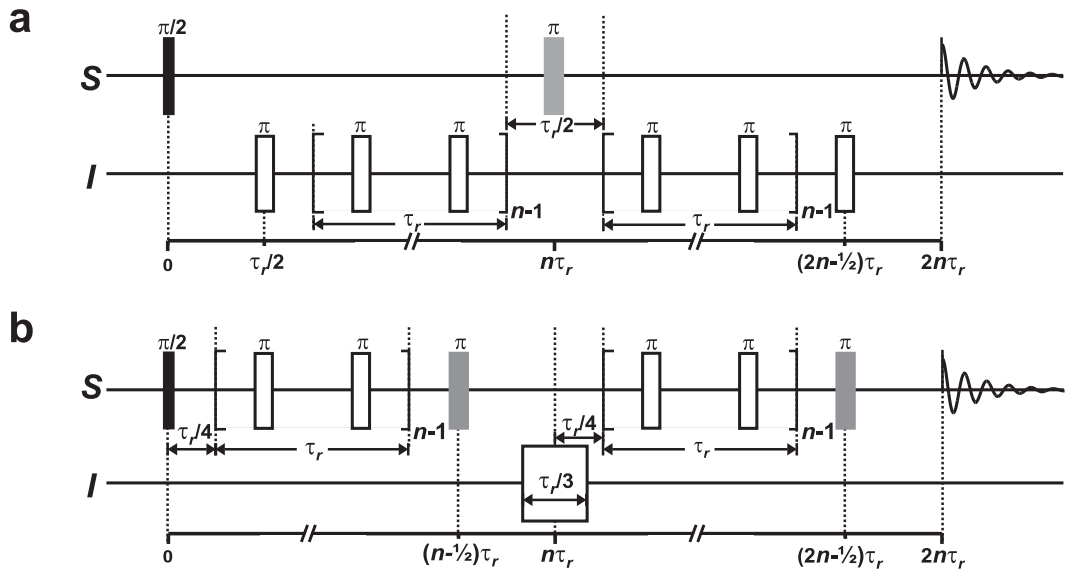

Fig. S1. Radio-frequency (rf) pulse schemes utilized for acquiring the (a) ^{23}Na$\{^{31}$P$\}$ REDOR and (b) ^{31}P$\{^{23}$Na$\}$ REAPDOR NMR data [S11,S21]. Solid black rectangles and open/grey rectangles represent $\pi/2$ and π-pulses, respectively. The grey rectangles mark pulses with fixed positions, regardless of the choice of the duration of the recoupling period; they are responsible for refocusing S-spin isotropic chemical shifts. The number of recoupling π-pulses (open rectangles) is incremented in blocks of 4 pulses that together span two rotational periods. This is commensurate with $\tau_{\mathrm{rec}}=2n\tau_r$ and n=1, 2, 3, ...

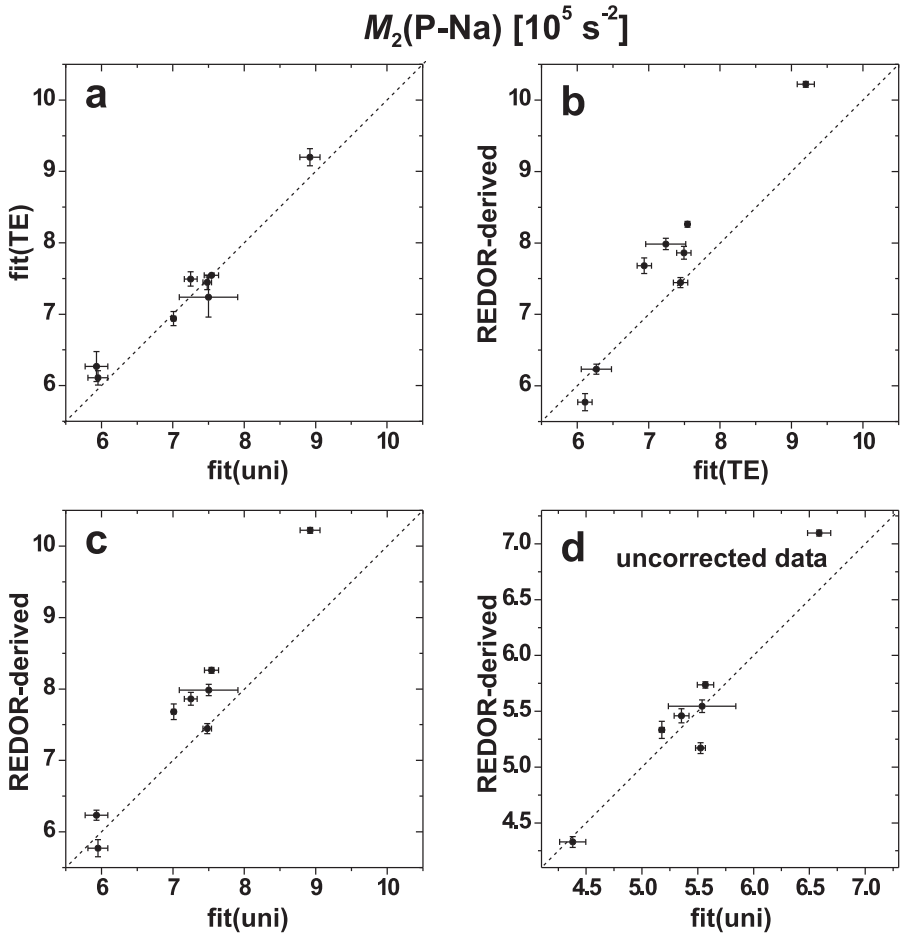

Fig. S2. Comparisons between various independent M_2(P–Na) estimates from the phosphosilicate glasses, where each dotted line indicates the result of a perfect agreement. Note that all plotted M_2-values were corrected (see sections **S2** and **S3**), except for those shown in (d) that represents the directly extracted best-fit results. (a) Second moments obtained by fitting the ^{31}P{^{23}Na} REAPDOR NMR results to Eqs. (S1) and (S2), shown along the vertical and horizontal axes, respectively. (b-d) Comparison between the REDOR-derived M_2(P–Na) values obtained from Eq. (2) and each directly determined ^{31}P{^{23}Na} REAPDOR counterpart.

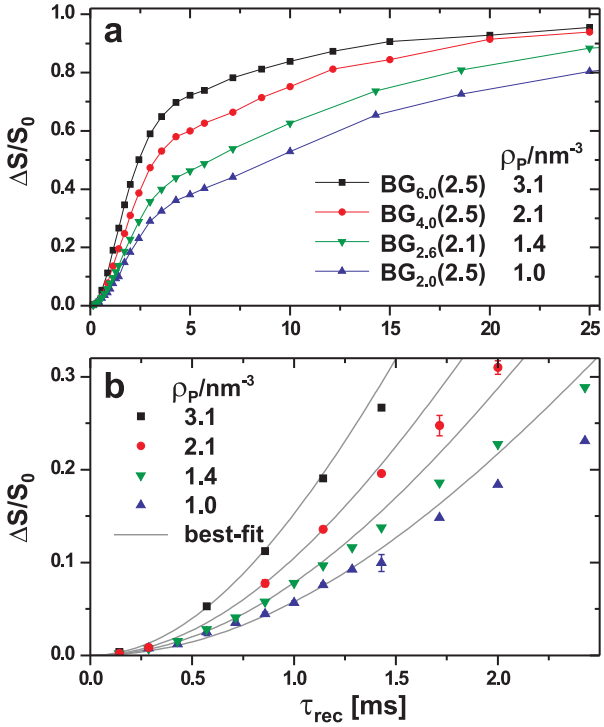

Fig. S3. (a) A selection of ^{23}Na{^{31}P} REDOR NMR dephasing curves ($\Delta S/S_0$ plotted against τ_{rec}) recorded from the Na_2O–CaO–SiO_2–P_2O_5 glasses. The data was acquired by using the pulse scheme shown of Fig. **S1**(a). Note that the dipolar dephasing increases concurrently with the number density of P in the structure. (b) Zoom of the initial dephasing regime, where the grey lines represent best-fit results to Eq. (S1) of the data spanning $\Delta S/S_0 \leq 0.10$. Error bars of the experimental data that are within the symbol sizes are not shown.

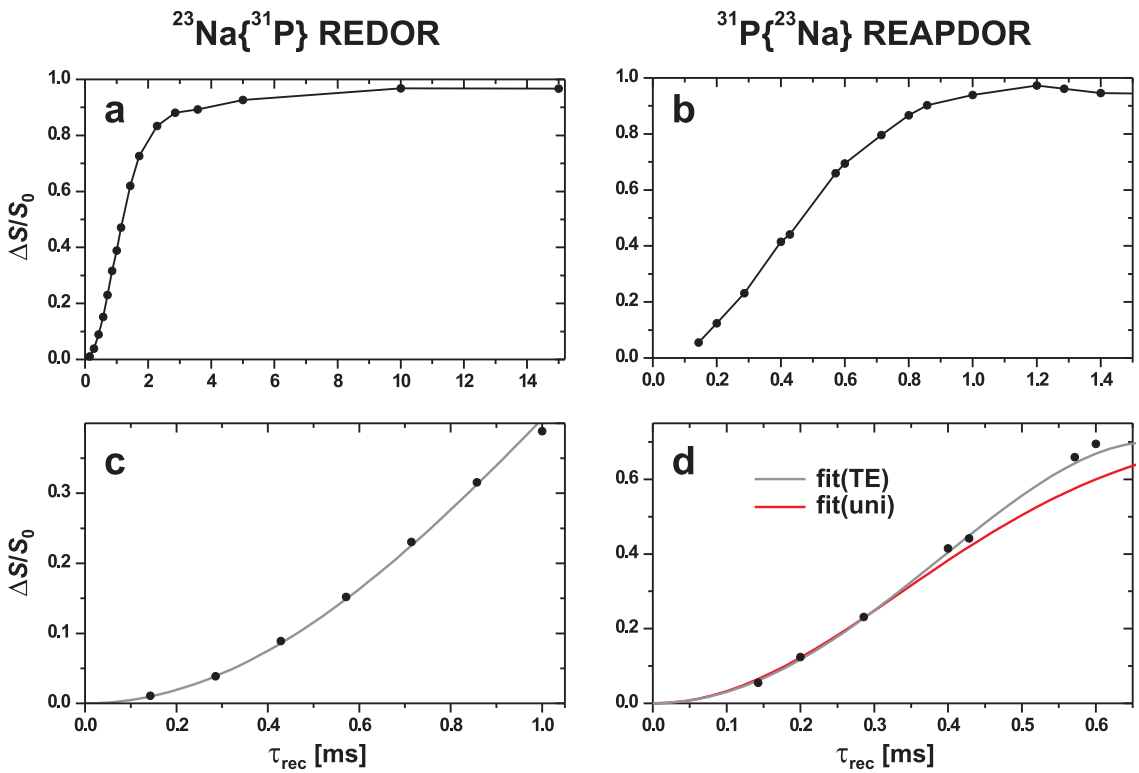

Fig. S4. ^{23}Na{^{31}P} REDOR (left panel) and ^{31}P{^{23}Na} REAPDOR (right panel) dipolar dephasing data recorded at B_0=9.4 T and 14.0 kHz MAS from a polycrystalline powder of Na_3PO_4. Complementary REAPDOR data was also obtained at ν_r=10.0 kHz. The plots in (c) and (d) are zooms of the initial dephasing regime of the plots in (a) and (b), respectively. The grey curve in (c) represents the best-fit to Eq. (S1), resulting in M_2^{exp}(Na–P)=9.03·10^4 s^{-2}. The corresponding value calculated from the XRD-derived structure is M_2^{XRD}(Na–P)=13.0·10^4 s^{-2} (see Table **S2**). The grey curve in (d) was utilized for determining the coefficient A=0.687 in Eq. (S1); this value was subsequently employed in the fitting of all other REAPDOR results (see section **S3**). The red curve in (d) resulted from fitting the data to Eq. (S2), yielding M_2^{exp}(P–Na)=1.46·10^6 s^{-2}, which may be compared with the result M_2^{XRD}(P–Na)=1.97·10^6 s^{-2}. All experimental errors are within the size of the symbols.

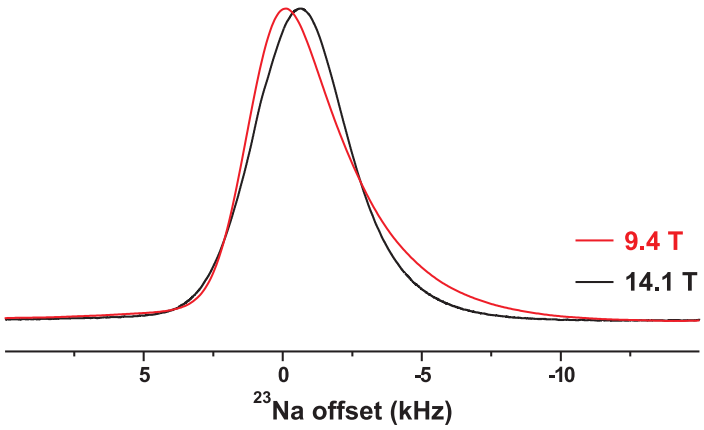

Fig. S5. ^{23}Na MAS spectra recorded from the glass sample $BG_{6.0}(2.5)$ (see Table **S1**) at external fields of B_0=9.4 T (red trace) and B_0=14.1 T (black trace) at the MAS rates of 14.0 kHz (4 mm MAS probehead) and 24.0 kHz (3.2 mm MAS probehead), respectively. The NMR acquisitions were otherwise very similar: they involved short rf pulses (0.5 μs) with ν_1^{Na} ≈80 kHz, and spectral windows and relaxation delays of 400 kHz and 2 s, respectively. Note the similar full width at half maximum (fwhm) peak-widths observed at both B_0 values, indicating that the reduced broadening from the second-order quadrupolar interaction at 14.1 T is offset by the accompanying higher chemical-shift dispersion. The main distinctions among the NMR spectra are manifested in the shifted peak-maximum observed at B_0=9.4 T and the correspondingly more pronounced "tailed" signal towards lower ppm-values. Besides slight shifts in the peak maxima, all ^{23}Na MAS NMR spectra acquired from the entire series of phosphosilicate glasses are essentially identical (not shown).

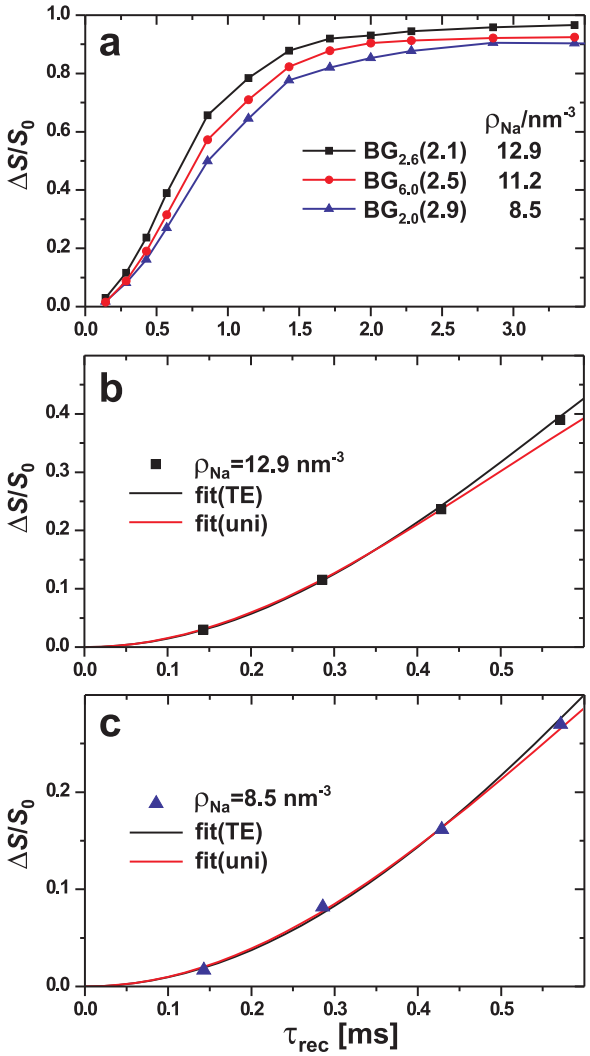

Fig. S6. (a) A selection of ^{31}P{^{23}Na} REAPDOR NMR dephasing curves acquired by the rf pulse scheme displayed in Fig. **S1**(b) from the as-indicated phosphosilicate glasses. The signal dephasing ($\Delta S/S_0$) rate increases together with the number density of Na in the glass. (b, c) Zoom of the initial dephasing regime for the two glasses featuring the (b) fastest and (c) slowest dephasing, respectively. The curves represent best-fit results to Eq. (S1) [black trace] and Eq. (S2) [red trace] when including the range $\Delta S/S_0 \lesssim 0.20$ in the numerical fitting. All experimental errors are within the size of the symbols.

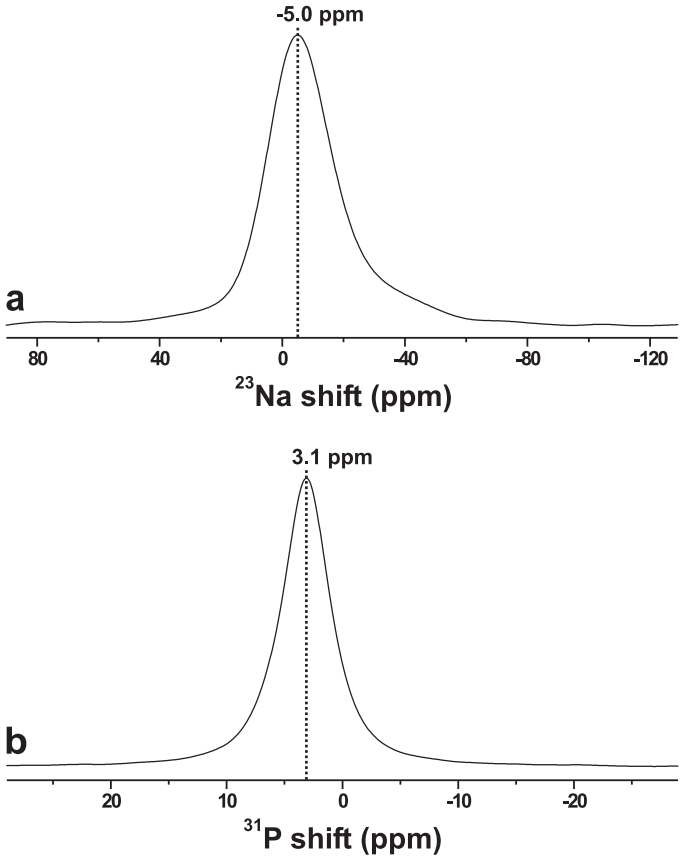

Fig. S7. (a) ^{23}Na and (b) ^{31}P MAS NMR spectra acquired from the S90sbf specimen at B_0=9.4 T with CT-selective single pulses (ν_r=14.0 kHz) and ^{1}H→^{31}P cross-polarization (ν_r=7.0 kHz), respectively.

References

[S1] R. Mathew, B. Stevensson, A. Tilocca, M. Edén, Toward a rational design of bioactive glasses with optimal structural features: Composition-structure correlations unveiled by solid-state NMR and MD simulations, J. Phys. Chem. B 118 (2014) 833–844.

[S2] B. Stevensson, R. Mathew, M. Edén, Assessing the phosphate distribution in bioactive phosphosilicate glasses by ^{31}P solid-state NMR and MD simulations, J. Phys. Chem. B 118 (2014) 8863–8876.

[S3] P. N. Gunawidjaja, R. Mathew, A. Y. H. Lo, I. Izquierdo-Barba, A. García, D. Arcos, M. Vallet-Regí, M. Edén, Local structures of mesoporous bioactive glasses and their surface alterations in vitro: inferences from solid state nuclear magnetic resonance, Phil. Trans. R. Soc. A 370 (2012) 1376–1399.

[S4] T. Gullion, D. B. Baker, M. S. Conradi, New, compensated Carr-Purcell sequences, J. Magn. Reson. 89 (1990) 479–484.

[S5] R. Mathew, P. N. Gunawidjaja, I. Izquierdo-Barba, K. Jansson, A. García, D. Arcos, M. Vallet-Regí, M. Edén, Solid state ^{31}P and ^{1}H NMR investigations of amorphous and crystalline calcium phopshates grown biomimetically from a mesoporous bioactive glass, J. Phys. Chem. C 115 (2011) 20572–20582.

[S6] Z. Yao, H.-T. Kwak, D. Sakellariou, L. Emsley, P. J. Grandinetti, Sensitivity enhancement of the central transition NMR signal of quadrupolar nuclei under magic-angle spinning, Chem. Phys. Lett. 327 (2000) 85–90.

[S7] W. Smith, T. R. Forester, DL_POLY_2.0: A general-purpose parallel molecular dynamics simulation package, J. Mol. Graphics 14 (1996) 136–141.

[S8] I. T. Todorov, W. Smith, K. Trachenko, M. T. Dove, DL_POLY_3: New dimensions in molecular dynamics simulations via massive parallelism, J. Mater. Chem. 16 (2006) 1911–1918.

[S9] A. Tilocca, A. N. Cormack, Structural effects of phosphorus inclusion in bioactive silicate glasses, J. Phys. Chem. B 111 (2007) 14256–14264.

[S10] W. Strojek, M. Kalwei, H. Eckert, Dipolar NMR strategies for multispin systems involving quadrupolar nuclei: ^{31}P{^{23}Na} rotational echo double resonance (REDOR) of crystalline sodium phosphates and phosphate glasses, J. Phys. Chem. B 108 (2004) 7061–7073.

[S11] H. Eckert, S. Elbers, J. D. Epping, M. Janssen, M. Kalwei, W. Strojek, U. Voigt, Dipolar solid state NMR approaches towards medium-range structure in oxide glasses, Topics Curr. Chem. 246 (2005) 195–233.

[S12] K. T. Mueller, Analytic solutions for the time evolution of dipolar-dephasing NMR signals, J. Magn. Reson., Ser. A 113 (1995) 81–93.

[S13] M. Bertmer, H. Eckert, Dephasing of spin echoes by multiple heteronuclear dipolar interactions in rotational echo double resonance NMR experiments, Solid State NMR 15 (1999) 139–152.

[S14] J. C. C. Chan, H. Eckert, Dipolar coupling information in multispin systems: Application of a compensated REDOR NMR approach to inorganic phosphates, J. Magn. Reson. 147 (2000) 170–178.

[S15] K. Nishimura, R. Fu, T. A. Cross, The effect of rf inhomogeneity on heteronuclear dipolar recoupling in solid state NMR: Practical performance of SFAM and REDOR, J. Magn. Reson. 152 (2001) 227–233.

[S16] E. Lissel, M. Jansen, E. Jansen, G. Will, Bestimmung der kristallstruktur von T-Na_3PO_4 mit röntgen- und neutronenpulvertechniken, Z. Kristallogr. 192 (1990) 233–243.

[S17] R. J. Harrison, A. Putnis, W. Kockelmann, Phase transition behaviour and equilibrium phase relations in the fast-ion conductor system Na_3PO_4–Na_2SO_4, Phys. Chem. Chem. Phys. 4 (2002) 3252–3259.

[S18] M. Catti, G. Ferraris, Hydrogen bonding in the cristalline state. NaH_2PO_4, a crystal structure with a short asymmetrical hydrogen bond, Acta. Cryst. B30 (1974) 1–6.

[S19] R. N. P. Choudhary, R. J. Nelmes, K. D. Rouse, A room-temperature neutron-diffraction study of NaH_2PO_4, Chem. Phys. Lett. 78 (1981) 102–105.

[S20] T. Gullion, Measurement of dipolar interactions between spin-1/2 and quadrupolar nuclei by rotational-echo, adiabatic-passage, double-resonance NMR, Chem. Phys. Lett. 246 (1995) 325–330.

[S21] T. Gullion, A. J. Vega, Measuring heteronuclear dipolar couplings for I=1/2, S>1/2 spin pairs by REDOR and REAPDOR NMR, Prog. NMR Spectrosc. 47 (2005) 123–136.

[S22] E. Nimerovsky, A. Goldbourt, Distance measurements between boron and carbon at natural abundance using magic angle spinning REAPDOR NMR and a universal curve, Phys. Chem. Chem. Phys. 14 (2012) 13437–13443.

[S23] M. Edén, The split network analysis for exploring composition-structure correlations in multi-component glasses: I. Rationalizing bioactivity-composition trends of bioglasses, J. Non-Cryst. Solids 357 (2011) 1595–1602.